NANO LETTERS

Letter

pubs.acs.org/NanoLett

Temporal Dynamics of Localized Exciton–Polaritons in Composite Organic–Plasmonic Metasurfaces

Elad Eizner,[*,†,§] Katherine Akulov,[‡,§] Tal Schwartz,[*,‡,§] and Tal Ellenbogen[*,†,§]

[†]Department of Physical Electronics, Fleischman Faculty of Engineering, [‡]School of Chemistry, Raymond and Beverly Sackler Faculty of Exact Sciences, and [§]Center for Light–Matter Interaction, Tel Aviv University, Tel Aviv 69978, Israel

Supporting Information

ABSTRACT: We use femtosecond transient absorption spectroscopy to study the temporal dynamics of strongly coupled exciton–plasmon polaritons in metasurfaces of aluminum nanoantennas coated with J-aggregate molecules. Compared with the thermal nonlinearities of aluminum nanoantennas, the exciton–plasmon hybridization introduces strong ultrafast nonlinearities in the composite metasurfaces. Within femtoseconds after the pump excitation, the plasmonic resonance is broadened and shifted, showcasing its high sensitivity to excited-state modification of the molecular surroundings. In addition, we observe temporal oscillations due to the deep subangstrom acoustic breathing modes of the nanoantennas in both bare and hybrid metasurfaces. Finally, unlike the dynamics of hybrid states in optical microcavities, here, ground-state bleaching is observed with a significantly longer relaxation time at the upper polariton band.

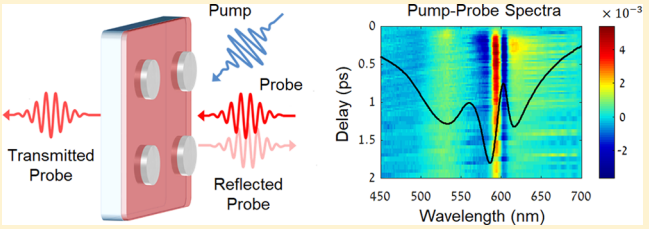

KEYWORDS: *Plasmonics, strong coupling, ultrafast photonics, organic polaritons, aluminum nanoantennas, temporal dynamics*

Optical cavities can have a strong effect on the interaction between light and matter due to modifications of the local density of photonic states. Hence, engineered cavity design can be used to obtain faster energy transfer between quantum emitters, e.g., atoms, molecules, quantum dots, or color centers in diamond, and electromagnetic (EM) fields, leading to a variety of interesting physical phenomena. In the weak coupling regime, the presence of cavities leads to brighter spontaneous emission, also known as the Purcell effect.[1−4] However, in the strong coupling regime, where the rate of energy transfer between the quantum emitters and EM modes is faster than their individual uncoupled decay, the presence of cavities gives rise to the formation of hybrid states with mixed properties of light and matter.[5,6]

Novel applications based on such hybrid light–matter states are now emerging. These include low-threshold polariton lasing,[7−9] ultrafast switching,[10,11] parametric amplification of optical signals,[12] nanoscale quantum devices,[13,14] and the modifications of energy-transfer pathways and chemical reactions.[15−20] Many of these applications require subwavelength confinement and control of the EM fields. Such confinement can be achieved in a variety of nanophotonic systems and specifically by using plasmons in metallic nanoparticles.[13,14,21−27]

Optical excitation of metallic nanoparticles at their localized surface plasmon (LSP) resonance results in strong scattering and absorption of light and in enhancement of the EM fields close to the metal surface.[28,29] As a result, metal nanoparticles can be used as antennas that focus light on the nanoscale and act as nano-optical cavities without the need for external mirrors. When quantum emitters are placed within the plasmonic mode volume, they can interact with the EM near-fields associated with the LSPs. Even when no plasmons are excited in the cavity, vacuum EM field fluctuations can manipulate the transitions of the quantum emitters.[30]

Among the plasmonic materials of choice, aluminum (Al) has emerged recently as a very attractive material for numerous applications.[24,31−36] Because the interband transition of Al exists only at a narrow energy band around 1.5 eV, the LSP modes supported by Al nanoparticles can have sufficiently high quality factors and large optical cross-sections over the entire visible region up to ultraviolet frequencies. Furthermore, Al is cheap, abundant, and forms a 2−3 nm stable oxide (Al_2O_3) layer almost immediately on exposure to air. This layer protects and preserves the nanoparticles, giving them long-term durability.[31]

Previously, we have shown[24] that metasurfaces of Al nanoantennas coated with molecular J-aggregates enable the formation of strongly coupled localized exciton–plasmon polaritons (X-LSP) at room temperature.[24] These metasurfaces can be engineered to control the polarization of the hybrid states and to decrease their mode volume. However, their optical nonlinearities and temporal dynamics, which can be extremely important for technological applications, are still not well-understood. Here, to bridge this gap, we use femtosecond transient absorption (TA) spectroscopy to study X-LSPs in

Received: August 31, 2017
Revised: October 22, 2017
Published: October 27, 2017

DOI: 10.1021/acs.nanolett.7b03751
Nano Lett. 2017, 17, 7675−7683

such composite Al−molecular metasurfaces. We first study the linear optical properties of the uncoupled and hybrid systems and then proceed to study their nonlinear dynamics. To analyze the complex TA results, we use a transient coupled harmonic oscillator (THO) model (see the Methods section) that captures some of the key physical processes of the nonlinear and temporal dynamics. We show that the nanoscale plasmonic confinement in metallic nanoparticle cavities introduces novel ultrafast phenomena in the strong coupling regime. These include modifications of the hybrid system due to femtosecond changes in the molecular environment, picosecond oscillations due to acoustic breathing modes of the nanoantennas, and long relaxation times of the nonlinear perturbation at the upper X-LSPs frequency band.

Experiment and Results. *Linear Optical Properties of the Bare Subsystems.* As our LSP platform, we studied metasurfaces composed of arrays of Al nanoantennas in the form of nanodisks on top of an indium tin oxide (ITO)-coated glass slide. Each array had a different disk diameter, D, ranging from 95 to 205 nm, and a fixed side-to-side separation, Γ, which was ∼190 nm. The nanoantennas were all 40 nm high, and the area of each of the arrays was 0.5 mm × 0.5 mm. The nanoparticle sizes and the separation distances are such that the resonances in each array are determined by the LSP resonances of individual nanoparticles.[21,24] A relatively large area was used to make sure that the probe beam remained entirely within the sample borders during the transient pump−probe experiments. A scanning electron microscope (SEM) image of one of the nanodisk arrays (D = 125 nm) is shown in Figure 1a. Figure 1b shows the measured spectral transmission through nanodisk arrays of varying disk diameters. The corresponding reflection measurements are shown in Figure S1. The dips in the transmission (or peaks in the reflection) correspond to light coupling to LSPs and the modification of the spectral position reveals the size-dependent dispersion of the LSPs. Figure 1c shows the linear relationship between the LSP resonance and the nanodisk diameter. The results show that nanoantennas that operate at optical frequencies follow linear design rules, as was shown previously.[37,38]

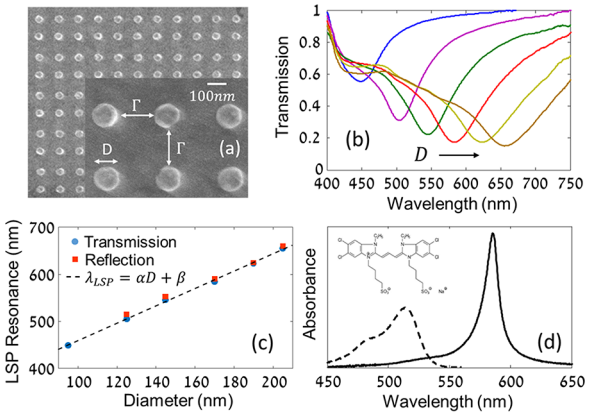

Figure 1. Linear optical properties of the bare subsystems. (a) SEM image of a sample of nanodisks with D = 125 nm and Γ = 190 nm. (b) Normalized transmission spectra of bare nanodisk arrays. The nanodisk diameter of each array is D = 95, 125, 145, 170, 190, and 205 nm. (c) Localized surface plasmon (LSP) resonance vs nanodisk diameter showing a linear dependence of $\lambda_{LSP} = \alpha D + \beta$ with α = 1.85 and β = 273. (d) Absorbance spectra of TDBC monomer (dashed line) and of TDBC J-aggregates (solid line) in aqueous solution. The inset shows the chemical formula of TDBC.

For the excitonic material in this study we used thin films of TDBC molecules (see the Methods section). The absorption spectrum of a low concentration of 10 μM TDBC monomers in aqueous solution is shown in Figure 1d as a dashed line. It is composed of a broad asymmetric band with a peak at 2.41 eV (514 nm) and a fwhm of 185 meV. At higher concentrations, TDBC forms linear chains of J-aggregating molecules.[39] The absorption spectrum of TDBC J-aggregates in an aqueous solution at a concentration of 9.84 mM, spin-coated on ITO-coated glass, is shown in Figure 1d as a solid line. The J-band absorption peak is at 2.12 eV (585 nm) and has a narrow line width of 53 meV. The red shift and narrowing of the absorbance resonance is due to the intermolecular coupling between the molecules, which causes delocalization of the electronic excitations on the aggregate.[40]

Linear Optical Properties of the Hybrid System. To study the behavior of hybrid states, the nanodisk metasurfaces were spin-coated with a thin layer of molecular J-aggregates. Figure 2a shows the measured transmission spectra through the coated arrays with varying disk diameters. For each array we observe two dips corresponding to a hybrid lower and upper X-LSPs states of the strongly coupled system and a dip at 585 nm, which corresponds to absorption due to uncoupled J-aggregate excitons in the area between the nanodisks (outside of the plasmonic mode volume). The resonance energies as a function of nanodisk diameter are shown in Figure 2b.

The experimental results were compared to a theoretical energy dispersion by[5,6,24]

$$E_{\mathrm{LP,UP}} = \frac{1}{2}\left[E_{\mathrm{X}} + fE_{\mathrm{LSP}} \pm \sqrt{(\hbar\Omega_{\mathrm{R}})^2 + (E_{\mathrm{X}} - fE_{\mathrm{LSP}})^2}\,\right] \quad (1)$$

where E_{X} and E_{LSP} are the uncoupled LSP and exciton energies and were taken from the experimental transmission dips of the uncoupled systems. The fitting parameters included the Rabi splitting $\hbar\Omega_{\mathrm{R}}$ and an additional parameter, f = 0.975, which takes into account the red shift to the bare LSPs resonances due to the change in the background dielectric constant after covering the samples with the J-aggregate dye layer. It can be seen that the experimental results agree very well with the model. A Rabi splitting of 0.3 eV was found from the energy dispersion, corresponding to an ultrafast periodic energy exchange between the excitons and LSP modes on a 14 fs time scale. A condition for strong coupling and Rabi splitting[6,24] is $\Omega_{\mathrm{R}} > \sqrt{\frac{\gamma_{\mathrm{X}}^2}{2} + \frac{\gamma_{\mathrm{LSP}}^2}{2}}$, where γ_{LSP} and γ_{X} are the uncoupled LSP and exciton decay rates, respectively. This condition is fulfilled in our experiments. Figure 2c shows a diagram of the bare and hybrid energy levels, including their vibronic manifolds, when the transitions $|X\rangle$ and $|LSP\rangle$ are in resonance. The upper and lower X-LSP states are marked by $|UP\rangle$ and $|LP\rangle$.

Nonlinear Optical Properties of the Bare Subsystems. Figure 3a shows the experimental TA spectrum of a thin layer of TDBC J-aggregates on ITO-coated glass. The pump wavelength in this case was 530 nm. The figure shows the relative change in transmission $\Delta T(\Delta t,\lambda)/T_0(\lambda) = [T(\Delta t,\lambda) - T_0(\lambda)]/T_0(\lambda)$, where T_0 and T are the transmission spectra without pump excitation and at a time delay Δt after pump excitation, respectively. The positive $\Delta T/T_0$ signal is a result of stimulated emission and ground-state bleaching (GSB), and

DOI: 10.1021/acs.nanolett.7b03751
Nano Lett. 2017, 17, 7675−7683

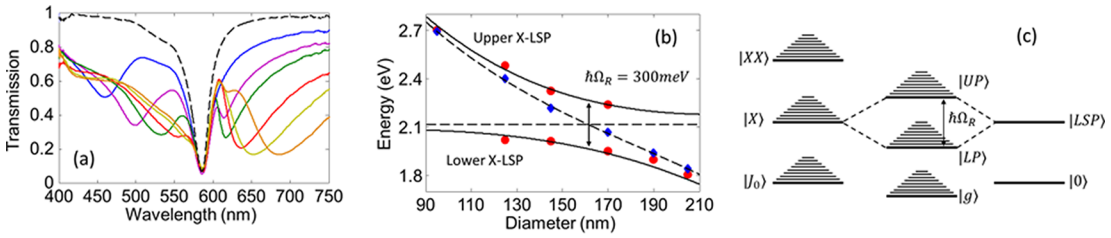

Figure 2. Linear optical properties of the hybrid system. (a) Normalized transmission spectra of TDBC J-aggregates-coated nanodisk arrays. The line colors correspond to the same nanodisk diameters as in Figure 1b (D = 95, 125, 145, 170, 190, and 205). (b) Energies of the transmission dips as a function of the diameter of the nanodisk array. Blue diamonds: bare nanodisk arrays (multiplied by the dielectric background correction factor). Red dots: nanodisk arrays coated with TDBC J-aggregates. Solid lines: theoretical fit. (c) Schematic diagram of the energy levels and the strong coupling between the molecular and plasmonic transitions $|X\rangle$ and $|LSP\rangle$, giving rise to new hybrid lower and upper polaritonic states $|UP\rangle$,$|LP\rangle$.

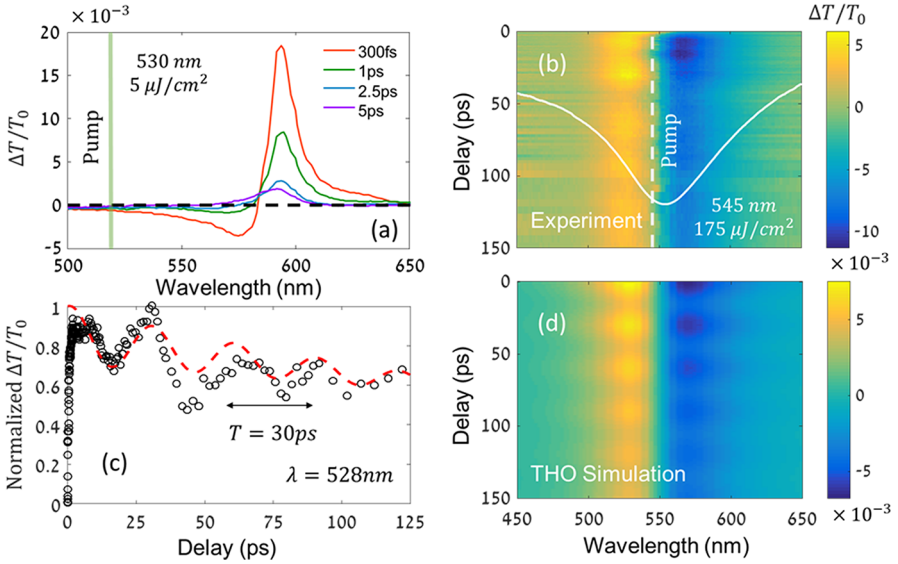

Figure 3. Transient absorption of the uncoupled subsystems. (a) Transient absorption spectra $\Delta T/T_0$ of a thin TDBC J-aggregate layer on indium tin oxide-coated glass, measured by the relative change in transmission upon excitation with a 530 nm pump pulse with fluence of 5 μJ/cm^2 and different pump−probe delay times. (b) Transient absorption spectra $\Delta T/T_0$ of aluminum nanodisk array with diameter D = 150nm upon close-to-resonance excitation with a 545 nm pump pulse with relatively high fluence of 175 μJ/cm^2 and different pump−probe delay times. The solid white line shows the linear transmission spectral shape. (c) Decay of the normalized $\Delta T/T_0$ signal at a probe wavelength of 528 nm showing 30 ps oscillations due to acoustic breathing modes of the nanodisks. The red dashed line is the corresponding normalized simulation result from the transient harmonic oscillator model (THO). (d) THO simulation with temporal resonance red shift and oscillations according to eqs 2 and 3.

corresponds to the creation of excited-state population at the single-exciton states. The blue-shifted negative $\Delta T/T_0$ signal is a result of excited state absorption (ESA) from the one-exciton state to the two-excitons state.[41] From a one-dimensional model of a homogeneous chain of molecules with nearest-neighbor interactions, it can be seen that the transition energy of the one exciton to two exciton state is larger than the energy of the one exciton state. This blue shift can be used to calculate the coherence size of the J-aggregate excitons[41,42] (see the Supporting Information). We used low pump fluence (5 μJ/cm^2) to avoid exciton−exciton annihilation effects[43] and photodegradation, and we verified that the transient spectra and relaxation lifetimes did not change with the pump intensity around this value. We observed that the pump-induced nonlinearities of the J-aggregate thin layer occur very rapidly and reach a maximum 300 *fs* after excitation. The positive bleach signal has a multiexponential decay with an initial decay time of 0.85 ps followed by a longer decay time of several picoseconds. Note that monomer traces were not observed in the linear or nonlinear spectral measurements of the J-aggregates. From our linear and nonlinear measurements, we estimate the coherent size of the J-aggregate excitons in our experiments to be spread over ∼10 molecules (see the Supporting Information).

Figure 3b shows the nonlinear $\Delta T/T_0$ signal of a bare nanodisk metasurface with a disk diameter D = 150 nm and an LSP resonance at 554 nm. The sample was excited using a pump pulse close to the LSP resonance at a wavelength of 545 nm with a fluence of 175 μJ/cm^2. This gave relatively weak optical nonlinearities with respect to the pump fluence. The nonlinearities appeared around the LSP resonance and reached maximal magnitude after a few picoseconds, followed by a slow decay lifetime of several hundreds of picoseconds and strong temporal oscillations with a period of ∼30 ps (Figure 3c). The observed oscillations are due to the creation of acoustic breathing modes in the disks by plasmon-induced thermal expansion. Such acoustic breathing modes in nanostructures have been studied mostly using gold,[44−47] but very recently also with Al nanodisks.[48] It was shown that there are substantial differences in the thermal nonlinearities between Al and gold nanodisks[48] with the TA signal of Al nanodisks an order of magnitude smaller than that of gold nanodisks. Another

DOI: 10.1021/acs.nanolett.7b03751
Nano Lett. 2017, 17, 7675−7683

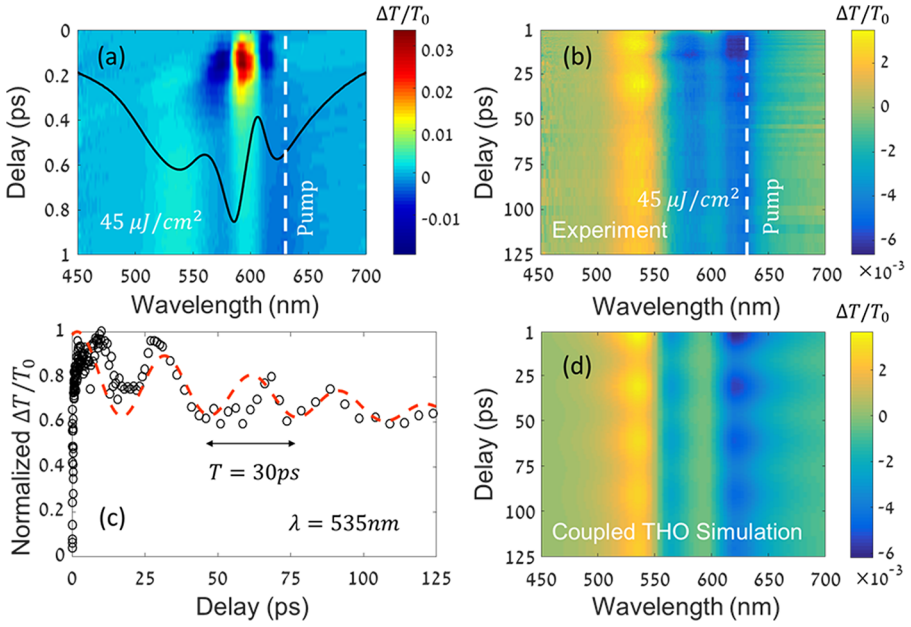

Figure 4. Transient absorption spectra of J-aggregate-coated nanodisk arrays with disk diameter of D = 155 nm, measured by the relative change in transmission upon excitation with a 630 nm pump pulse with fluence of 45 μJ/cm^2 and pump−probe delay times between (a) 0−1 ps and (b) 1−125 ps. The solid black line shows the corresponding linear transmission spectral shape of the studied sample before the pump−probe measurement. (c) Decay of the normalized $\Delta T/T_0$ signal at a probe wavelength of 535 nm exhibiting 30 ps oscillations due to acoustic breathing modes of the nanodisks. The red dashed line shows the coupled THO model simulation. (d) Coupled THO simulation with temporal resonance red shift and oscillations according to eqs 2 and 3.

difference was that the fast, initial relaxation due to electron−phonon coupling seen in gold was not apparent in Al. In addition, the acoustic vibrations in Al nanodisks were shown to be affected by the native Al oxide layer.

Using a THO model (see the Methods section) with a pump-induced red shift of the LSP resonance ω^0_{LSP} gives:

$$\omega_{LSP}(I_{pump}, \Delta t) \rightarrow \omega^0_{LSP} - \Delta\omega(I_{pump}, \Delta t) \quad (2)$$

and

$$\Delta\omega(I_{pump}, \Delta t) = \Delta\omega_a \cdot e^{-\Delta t/\tau_a} + \Delta\omega_b \cdot e^{-\Delta t/\tau_b} \cdot \cos\left(\frac{2\pi\Delta t}{T} - \phi\right) \quad (3)$$

where the first term in eq 3 corresponds to the cooling of the nanodisk with a decay time of τ_a = 390 ps, which is the time required for the thermal exchange between the Al lattice and the environment. The second term in eq 3 corresponds to the acoustic breathing mode with a decay time of τ_b = 100 ps, which results from the acoustic energy dissipation to the local environment. $\Delta\omega_a$ = 1.04 meV, and $\Delta\omega_b$ = 0.18 meV are the frequency shift amplitudes, T = 30 ps is the oscillation period, and $\phi = 0.08\pi$ is the oscillation phase. We can then further relate the temporal oscillations of the resonance to expansion of the nanodisk due to acoustic vibrations. Using eq 3 together with the observed linear relation between the nanodisk diameter and the LSP resonance $\lambda_{LSP} = \alpha D + \beta$ (see Figure 1c) and $\Delta\lambda/\lambda_{LSP} = \Delta\omega/\omega_{LSP}$, the maximal expansion of the diameter of the nanodisk as a result of the pump pulse is calculated to be:

$$\Delta D_{max} \approx \frac{\lambda_{LSP}}{\alpha\omega_{LSP}}\Delta\omega_b = 0.025\ \text{nm} \quad (4)$$

The simulated dynamics, based on the THO model with the above parameters, are shown in Figure 3d and clearly reproduce the experimental data (Figure 3b). These results demonstrate that TA spectroscopy, combined with the relationship between nanoparticle geometry and LSP resonance, can be used to measure subangstrom electro-mechanic volume modifications. This method has potential use for nanostructures in emerging optomechanical applications, e.g., photoacoustic imaging,[49] mass sensing,[50] or as nanomechanical resonators.[51]

Nonlinear Optical Properties of the Hybrid System. To study the temporal dynamics of the hybrid states and their optically induced nonlinearities, we performed extensive TA spectroscopy analysis of the TDBC J-aggregate-coated nanodisk arrays. To reveal the effects of the excited-states dynamics, our study included arrays with different disk diameters corresponding to detuning between the bare LSP and exciton resonance energies and pump excitation at different energies.

Initially, we evaluated the TA results for the case of a pump pulse tuned to the lower polariton (λ = 630 nm) of the composite sample of nanodisk array with a disk diameter of D = 155 nm (Figure 4). At low pump fluences of 5 μJ/cm^2, such as the ones used to pump the bare J-aggregate sample, no nonlinear signal was observed at the polariton wavelengths. However, when we increased the pump fluence significantly (45 μJ/cm^2), a $\Delta T/T_0$ signal above the noise level at polariton wavelengths was observed. Figure 4a focuses on delay times of 0−1 ps, where the nonlinear signal around the uncoupled J-aggregates band appears distorted, decays very rapidly and does not resemble the TA signals obtained with low pump fluences. This could be due to nonlinear effects such as exciton−exciton annihilation.[43] Figure 4b shows the dynamics between 1−125 ps, where thermal and acoustic effects dominate the nonlinear signal in a similar manner to the bare nanoantenna samples. The results show three slowly decaying spectral bands, one with a positive $\Delta T/T_0$ signal and the other two with a negative $\Delta T/T_0$ signal. As presented in Figure 4c, the decay of the

DOI: 10.1021/acs.nanolett.7b03751
Nano Lett. 2017, 17, 7675−7683

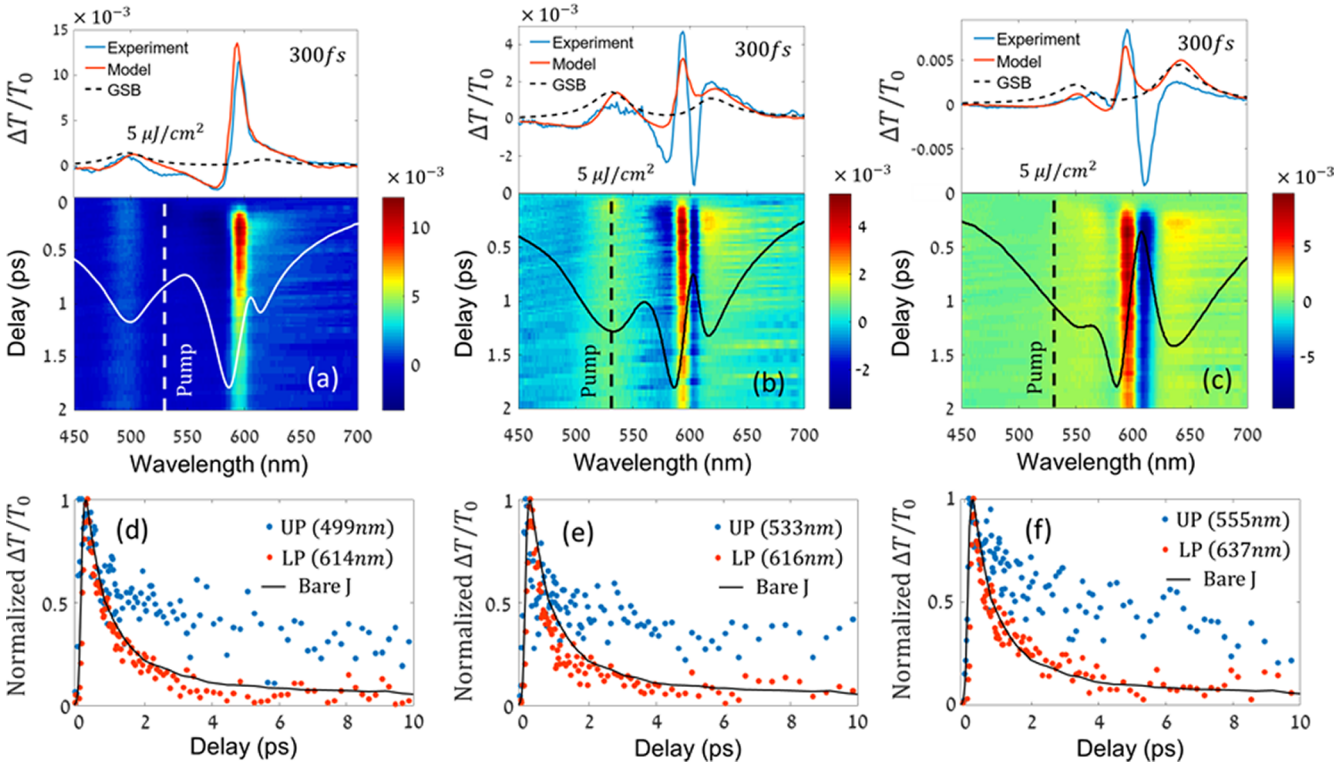

Figure 5. Transient absorption spectra of J-aggregate-coated nanodisk arrays with disk diameter of (a) D = 125 nm, (b) D = 145 nm, and (c) D = 170 nm, measured by the relative change in transmission upon excitation with a 530 nm pump pulse with a fluence of 5 μJ/cm^2 and different pump−probe delay times. (a−c, top) The solid blue line shows the transient absorption spectrum for a delay time of 300 fs. The solid red line shows the coupled THO simulation, and the dashed black line shows the decrease of absorption and scattering of the hybrid modes in the coupled THO model marked as GSB. (a−c, bottom) Transient absorption spectra for pump−probe delay times of 0−2 ps. The solid white and black lines show the corresponding linear transmission spectral shape of the studied sample. (d−f) The corresponding normalized decay of $\Delta T/T_0$ signal for probe wavelengths as indicated in the figures. The solid black lines show the decay of a sample composed of only a thin TDBC J-aggregate layer at the GSB signal resonance for the same pump excitation.

normalized $\Delta T/T_0$ signal at a probe wavelength of 535 nm clearly shows temporal oscillations of 30 ps, similar to the oscillations of the bare Al metasurface (Figure 3). Figure 4d shows that the $\Delta T/T_0$ signal can be described well by a coupled THO model (see the Methods section) with a red shift of the LSP resonance. This can be done using eqs 2 and 3 with reduced coupling coefficient G (see the Methods section) due to high pump fluence induced damage to the aggregates. The resonance red shift decays with time constants of τ_a = 500 ps and τ_b = 80 ps, frequency shift amplitudes of $\Delta\omega_a$ = 0.836 meV and $\Delta\omega_b$ = 0.204 meV, an oscillation period of T = 30 ps, and a phase of $\phi = 0.15\pi$. Compared with the results of the bare nanodisk, the oscillation time period is found to be the same, and the values of the decay times τ_a and τ_b are also very close. The small differences could result from the effects of the molecular surrounding on the acoustic energy dissipation and on the thermal conductivity of the medium. To the best of our knowledge, this provides the first observation of the influence of acoustic nanoantenna breathing modes on hybrid light−matter states.

Figures 5a−c show the TA spectra for J-aggregate coated arrays with disk diameter of D = 125 nm, D = 145 nm, and D = 170 nm, respectively, using pump pulse excitation at a wavelength of 530 nm with a fluence of 5$\frac{\mu J}{cm^2}$ (single delay time line plots of the data are shown in Figure S4). The lower section of the figures shows the $\Delta T/T_0$ spectra for pump−probe time delays of 0−2 ps, and the top section shows the $\Delta T/T_0$ signal for a single time delay of 300 fs (blue lines). The figure shows that hybridization with excitons introduces strong ultrafast nonlinearities in the composite metasurfaces. The entire spectrum of the $\Delta T/T_0$ signal reaches a maximal magnitude after a mere ∼300 fs time delay between the pump and probe pulses, similar to the nonlinearity rise time that we observed in the J-aggregate thin layer (Figure 3a). The positive and negative $\Delta T/T_0$ signals at the vicinity of the J-aggregate spectral band are due to the uncoupled J-aggregate excitons. In addition, as can be seen in all three arrays, there are clear positive $\Delta T/T_0$ signals at the exact spectral locations of the linear transmission resonances of the upper and lower X-LSPs.

The experimental results can be described by using a coupled THO model (see the Methods section) with the following pump induced transient effects. A blue shift and broadening of the LSP resonance by $\omega_{LSP}(I_{pump},\Delta t) \rightarrow \omega^0_{LSP} + \Delta\omega_{LSP}(I_{pump},\Delta t)$, $\gamma_{LSP}(I_{pump},\Delta t) \rightarrow \gamma^0_{LSP} + \Delta\gamma_{LSP}(I_{pump},\Delta t)$ and a decrease in the absorption and scattering of the hybrid modes by $A_{\sigma,c}(I_{pump},\Delta t) \rightarrow A^0_{\sigma,c} - \Delta A_{\sigma,c}(I_{pump},\Delta t)$. Note that we also included contributions from uncoupled J-aggregates to the nonlinear spectra (see the Methods section). The coupled THO model results are shown in the top curves in Figure 5a−c as red lines. A decrease of the parameter $A_{\sigma,c}$ in the coupled THO model corresponds to the experimental GSB and is shown as dashed black lines. The LSP resonance blue shifts by $\Delta\omega_{LSP}$ = 0.15 meV, and the resonance is broadened by $\Delta\gamma_{LSP}$ = 0.3 meV. The decrease in absorption we found is $\Delta A_{\sigma,c}$ = 5 ×

DOI: 10.1021/acs.nanolett.7b03751
Nano Lett. 2017, 17, 7675−7683

10^{-4}, 4.5×10^{-4}, or 10^{-3} for arrays with disk diameter of D = 125, 145, or 170 nm, respectively.

We attribute the ultrafast change of the plasmonic resonance to the modification of the optical properties of the molecular surroundings as a result of the pump excitation. Note that the negative $\Delta T/T_0$ signal at probe wavelengths around 604 nm for Figure 5b or around 610 nm for Figure 5c are not represented very well by the model. This is due to the fact that the linear transmission lineshapes of X-LSPs and of the uncoupled molecules are not homogeneous[52] and cannot be described exactly with Lorentzian functions. As can be seen in Figure S2, there are differences in the sharp maximum features in the model fit to the linear transmission data, which affect the THO model results as well. Note that in the cases of Figures 5a and S3c, when the sharp features are less pronounced, the agreement between the experiment and the THO model is much better. Nevertheless, in Figure 5b,c, the qualitative trends agree very well. It is also important to note that the energy at which these negative $\Delta T/T_0$ signals appear does not match excited-state absorption to the XX state. Moreover, because we use low pump fluence, we do not find that the modification of the coupling strength G is responsible for the spectral transient absorption features as has been found in other systems.[10,11,53]

The normalized $\Delta T/T_0$ decay kinetics for probe wavelengths at the lower and upper polariton resonance are shown in Figure 5d–f. The signal at probe wavelengths corresponding to the lower X-LSP resonance decays in a similar way to the GSB of bare TDBC J-aggregates (shown as a black line). Remarkably, at a probe wavelength corresponding to the upper X-LSP resonance, the nonlinear signal decays much slower. The slow decay occurs when the pump energy is lower (Figure 5d and also in Figure S3), the same as (Figure 5e), or higher (Figure 5f) than the upper X-LSP resonance energy. As can be seen in Figure S5, a similar decay is also observed in measurements of the relative change in reflectance. As elaborated in the Discussion section, such a phenomenon was not observed in microcavity polaritons. Note that the $\Delta T/T_0$ signal in the spectral vicinity of the upper X-LSP resonance band decays faster than the positive $\Delta T/T_0$ signal at resonance. As shown by the model, this is due to a shift and broadening of the LSP resonance shape. The negative $\Delta T/T_0$ signal that appears at wavelengths shorter than the lower X-LSP resonance wavelengths in Figure 5b,c is attributed to similar effects.

Discussion. TA measurements were performed to unveil the complex behavior of the hybrid molecular X-LSPs states in composite metasurfaces. Our study is quantitative and permits the comparison of different nonlinear mechanisms. Importantly, the thermal nonlinearities of the aluminum metasurfaces were found to be much weaker and to have a completely different transient fingerprint than other nonlinear effects of the hybrid-states dynamics or the J-aggregates. This allowed us to study the photophysics of hybrid states directly.

We observe that the dynamics of the hybrid system goes far beyond the Rabi oscillations time scales. Observation in real time of the Rabi oscillations[11] is not manifested here because the ultrafast time period of the Rabi oscillation in our system is 14 fs, far below the temporal resolution of our measurement, which is dictated by the pump and probe pulse durations. The relaxation dynamics of the molecular and hybrid states also play an important role in the observation of Rabi splitting in photoluminescence, as was shown in recent studies using similar systems.[54,55] Interestingly, in these studies it was observed that the Rabi splitting in photoluminescence increased when the system was cooled to cryogenic temperatures.[54]

The coupled THO model that we use is shown to extract the key processes that influence the TA spectra. Using this model, we find that when the composite metasurfaces were excited by a pump pulse at higher energy than the J-aggregate absorption band, with a wavelength of either 530 nm (Figure 5) or 580 nm (Figure S3), the effect of the pump on the TA spectra is due to a broadening and a blue shift of the LSP resonance and the GSB of the upper and lower X-LSP bands. Because the modifications to the LSP resonance decay on a time scale similar to that of the uncoupled J-aggregates, we conclude that these effects are due to the LSP resonance sensitivity to pump-induced changes in the molecular medium that covers the metasurface. The decay behavior of the GSB signal of the lower X-LSP band is also very similar to the decay of the uncoupled J-aggregates, but surprisingly, the decay time of the GSB signal of the upper X-LSPs band was found to be much longer. Such slow upper polariton decay behavior was not previously reported in microcavity organic exciton–polaritons,[56–58] nanoparticles covered by J-aggregate shells in a solution,[53,59–61] or gold nanoslit arrays.[11,62,63] To the best of our knowledge, the only publication of a similar effect is a very recent report in a system composed of gold nanohole arrays covered by a 300 nm thick layer of J-aggregates embedded in a poly(vinyl alcohol) film.[64] In that paper, the slow upper polariton decay was attributed to a trapped state under upper-polariton excitation. Here, our comprehensive study shows that a slow decay also occurs when the pump energy is lower than the upper X-LSP resonance (Figure 5d and also Figure S3), ruling out the direct filling of the upper X-LSP states as the cause for the slow decay. Filling of the upper X-LSP states from higher-energy state transitions (e.g., from the XX level) is also less likely to be a dominant process because it would have to involve a two-photon absorption process, which is expected to be much weaker. It is reasonable to assume that this effect is due to the high sensitivity of plasmonic nanostructures to interactions with their molecular surrounding, which can alter the LSP resonance and possibly even modify the electronic relaxation pathways. In fact, it is well-known that metal nanoparticles are extremely sensitive to modifications close to the metal surface, which is the basis of surface plasmons sensing applications and the main cause for the breakthrough of the entire plasmonic field. Nevertheless, to fully reveal the origin of this unique phenomenon, additional extensive experimental and theoretical studies are required.

Conclusions. In this study, we observed novel and intriguing phenomena in the temporal dynamics of hybrid X-LSPs in the metasurfaces of Al nanoantennas coated with molecular J-aggregates. For pump excitations with a wavelength shorter than the uncoupled J-aggregate band, we found that the relaxation dynamics are mostly dominated by the uncoupled states. Using a transient coupled harmonic oscillator model, we analyzed the complex transient absorption spectra and found broadening and a shift of the plasmonic resonance and, notably, asymmetric relaxation times of the GSB signal for the lower and upper X-LSP bands, where the latter was found to be much longer. Moreover, we observed temporal oscillations due to acoustic breathing modes of the Al nanoantennas in the bare and hybrid systems. These effects result from the nanoscale plasmonic confinement in the nanoantennas and their interaction with the molecular surroundings.

DOI: 10.1021/acs.nanolett.7b03751
Nano Lett. 2017, 17, 7675–7683

Methods. *Sample Preparation.* A cleaned substrate of indium tin oxide coated glass was spin-coated with poly(methyl methacrylate) (PMMA), followed by baking at 180 °C on a hot plate for 1 min. The nanodisk arrays were written using an electron-beam lithography system (Raith 150) at 10 kV. The area of each array was 0.5 mm × 0.5 mm, and to reduce the writing time, we used a fixed-beam moving stage (FBMS) method. A 40 nm film of Al was evaporated at a rate of 1Å/s, followed by removal of any excess with acetone. The samples were then treated with oxygen plasma for 20 s, followed by spin coating at 2500 rpm with a solution prepared by sonicating 0.015 g of cyanine dye molecules (TDBC) in 2 g of DI water for 10 minutes. 5,6-Dichloro-2-[[5,6-dichloro-1-ethyl-3-(4-sulfobutyl)-benzimidazol-2-ylidene]-propenyl]-1-ethyl-3-(4-sulfobutyl)-benzimidazolium hydroxide (TDBC), inner salt, sodium salt) was purchased from Few Chemicals. The dimensions of the nanodisks were measured using a scanning electron microscope (SEM JSM-6700).

Optical Characterization. All measurements were performed at room temperature. Spectral transmission and reflection measurements were performed using an inverted microscope (Zeiss Axio Observer Z1m with 10×/0.25 objective and multicolor LED illumination), in transmission or reflection mode, respectively. The light was collected by a spectrometer (Andor, Shamrock 193i). Transient absorption spectroscopic measurements were performed using a commercial broadband pump−probe femtosecond system (HELIOS, Ultrafast Systems). The pump source was a pulsed femtosecond laser (Spitfire Ace, Spectra Physics; pulse width of 80 fs and repetition rate of 1 kHz) with a tunable wavelength OPA (Topas, Light Conversion). The probe was a white-light (400−800 nm) generated by a sapphire plate. The system was operated in transmission mode.

Transient Harmonic Oscillator Model. To analyze the TA spectra in our experiments, we modified an harmonic oscillator model[65−68] to include the nonlinear effects induced by the pump pulse. The transient harmonic oscillator (THO) equation of motion that describes the LSP can be written as:

$$\ddot{x}_{LSP} + \gamma_{LSP}(I_{pump}, \Delta t)\dot{x}_{LSP} + \omega^2_{LSP}(I_{pump}, \Delta t)x_{LSP} = F_{probe} \tag{5}$$

where $x_{LSP}(t) = x_{LSP}(0)e^{-i\omega t}$ represents the LSP charge displacement, ω_{LSP} is the resonance frequency, γ_{LSP} is the oscillator damping rate, $F_{probe}(t) = F_{probe}(0)e^{-i\omega t}$ is the external force of the probe EM field, I_{pump} is the pump fluence, and Δt is the time delay between pump and probe. The dissipated power is calculated by the work done by the external force over an optical cycle:

$$P(\omega, I_{pump}, \Delta t) = \int_0^{2\pi/\omega} \mathrm{Re}\{F_{probe}(t)\}\mathrm{Re}\{\dot{x}_{LSP}(t)\}\, dt \tag{6}$$

where Re{} is the real part. The transmission can be written as:

$$T(\omega, I_{pump}, \Delta t) = 1 - A_\sigma \frac{P(\omega, I_{pump}, \Delta t)}{\max\{P(\omega, I_{pump}, \Delta t)\}} \tag{7}$$

where A_σ is a constant factor that takes into account the absorption and scattering cross-sections of the nanoantennas. Finally, the TA signal is $(T(\omega, I_{pump}, \Delta t) - T_0)/T_0$, where T_0 is the calculated linear transmission without the pump (see Figure S2).

Transient Coupled Harmonic Oscillator Model. To analyze the TA spectra for the hybrid system in our experiments, we extended the previous model to account for the interaction between the excitons and LSPs.[65,69,70] The coupled THO equations of motion are:

$$\begin{aligned}\ddot{x}_{LSP} + \gamma_{LSP}(I_{pump}, \Delta t)\dot{x}_{LSP} + \omega^2_{LSP}(I_{pump}, \Delta t)x_{LSP} - G(I_{pump}, \Delta t)x_X &= F_{probe}\\ \ddot{x}_X + \gamma_X(I_{pump}, \Delta t)\dot{x}_X + \omega^2_X(I_{pump}, \Delta t)x_X - G(I_{pump}, \Delta t)x_{LSP} &= aF_{probe}\end{aligned} \tag{8}$$

where $x_X = x_X(0)e^{-i\omega t}$ represents the exciton charge displacement, ω_X is the resonance frequency, γ_X is the oscillator damping rate, and a is a constant factor to account for the different force felt by the excitons because of the probe EM field. Inside the volume of interaction, we assume that $\alpha \ll 1$. G is the coupling constant between the oscillators. The dissipated power of the coupled harmonic oscillators is:

$$P_c(\omega, I_{pump}, \Delta t) = \int_0^{2\pi/\omega} [\mathrm{Re}\{F_{probe}(t)\}\mathrm{Re}\{\dot{x}_{LSP}(t) + a\dot{x}_X(t)\}]\, dt \tag{9}$$

and the linear transmission is calculated by:

$$T(\omega, I_{pump}, \Delta t) = 1 - A_{\sigma,c}(I_{pump}, \Delta t)\frac{P_c(\omega, I_{pump}, \Delta t)}{\max(P_c(\omega, I_{pump}, \Delta t))} \tag{10}$$

where $A_{\sigma,c}$ is a factor that takes into account the absorption and scattering cross-sections of the hybrid states. This parameter can be modified by the pump due to GSB. To calculate the linear transmission spectra without the pump, we also included an additional uncoupled harmonic oscillator that corresponds to the uncoupled J-aggregates in our system (see Figure S2). Finally, the TA signal is calculated by $(T(\omega, I_{pump}, t) - T_0)/T_0$, and we also add experimental uncoupled J-aggregate TA data (from an experiment with the same pump wavelength and fluence) multiplied by constant factor a_x. In Figure 5, we used $a_x = 0.715$, 0.166, or 0.33 for arrays with disk diameters of D = 125, 145, or 170 nm, respectively.

■ ASSOCIATED CONTENT

Supporting Information

The Supporting Information is available free of charge on the ACS Publications website at DOI: 10.1021/acs.nanolett.7b03751.

Additional details and figures showing the estimation of the coherent size of J-aggregate excitons, reflection of bare nanodisk metasurfaces, linear transmission fits using a single or coupled harmonic oscillator models, transient absorption of the hybrid system for a pump at the J-band, single delay time line plots of the transient absorption data, pump−probe relative change in reflection, transient absorption of TDBC monomers. (PDF)

■ AUTHOR INFORMATION

Corresponding Authors

*E-mail: eladeiz@post.tau.ac.il.
*E-mail: talschwartz@post.tau.ac.il.
*E-mail: tellenbogen@tauex.tau.ac.il.

ORCID

Elad Eizner: 0000-0001-7603-6219

DOI: 10.1021/acs.nanolett.7b03751
Nano Lett. 2017, 17, 7675−7683

Notes

The authors declare no competing financial interest.

■ ACKNOWLEDGMENTS

This work was supported by the Israeli Science Foundation, grant no. 1331/13 and by the European Commission Marie Curie Career Integration grant no. 333821. We thank Ori Avayu, Lior Michaeli, and Dr. Yigal Lilach for useful discussions.

■ REFERENCES

(1) Purcell, E. *Phys. Rev.* **1946**, *69*, 681.
(2) Goy, P.; Raimond, J. M.; Gross, M.; Haroche, S. *Phys. Rev. Lett.* **1983**, *50*, 1903−1906.
(3) Anger, P.; Bharadwaj, P.; Novotny, L. *Phys. Rev. Lett.* **2006**, *96*, 113002.
(4) Liebermann, T.; Knoll, W. *Colloids Surf., A* **2000**, *171*, 115−130.
(5) Deng, H.; Haug, H.; Yamamoto, Y. *Rev. Mod. Phys.* **2010**, *82*, 1489−1537.
(6) Törmä, P.; Barnes, W. L. *Rep. Prog. Phys.* **2015**, *78*, 13901.
(7) Kéna-Cohen, S.; Forrest, S. R. *Nat. Photonics* **2010**, *4*, 371−375.
(8) Daskalakis, K. S.; Maier, S. A.; Murray, R.; Kéna-Cohen, S. *Nat. Mater.* **2014**, *13*, 271−278.
(9) Plumhof, J. D.; Stöferle, T.; Mai, L.; Scherf, U.; Mahrt, R. F. *Nat. Mater.* **2013**, *13*, 247−252.
(10) Vasa, P.; Pomraenke, R.; Cirmi, G.; De Re, E.; Wang, W.; Schwieger, S.; Leipold, D.; Runge, E.; Cerullo, G.; Lienau, C. *ACS Nano* **2010**, *4*, 7559−7565.
(11) Vasa, P.; Wang, W.; Pomraenke, R.; Lammers, M.; Maiuri, M.; Manzoni, C.; Cerullo, G.; Lienau, C. *Nat. Photonics* **2013**, *7*, 128−132.
(12) Saba, M.; Ciuti, C.; Bloch, J.; Thierry-Mieg, V.; André, R.; Dang, L. S.; Kundermann, S.; Mura, A.; Bongiovanni, G.; Staehli, J. L.; et al. *Nature* **2001**, *414*, 731−735.
(13) Chikkaraddy, R.; de Nijs, B.; Benz, F.; Barrow, S. J.; Scherman, O. A.; Rosta, E.; Demetriadou, A.; Fox, P.; Hess, O.; Baumberg, J. J. *Nature* **2016**, *535*, 127−130.
(14) Zengin, G.; Wersäll, M.; Nilsson, S.; Antosiewicz, T. J.; Käll, M.; Shegai, T. *Phys. Rev. Lett.* **2015**, *114*, 157401.
(15) Hutchison, J. A.; Schwartz, T.; Genet, C.; Devaux, E.; Ebbesen, T. W. *Angew. Chem., Int. Ed.* **2012**, *51*, 1592−1596.
(16) Hutchison, J. A.; Liscio, A.; Schwartz, T.; Canaguier-Durand, A.; Genet, C.; Palermo, V.; Samorì, P.; Ebbesen, T. W. *Adv. Mater.* **2013**, *25*, 2481−2485.
(17) Wang, S.; Mika, A.; Hutchison, J. A.; Genet, C.; Jouaiti, A.; Hosseini, M. W.; Ebbesen, T. W. *Nanoscale* **2014**, *6*, 7243−7248.
(18) Thomas, A.; George, J.; Shalabney, A.; Dryzhakov, M.; Varma, S. J.; Moran, J.; Chervy, T.; Zhong, X.; Devaux, E.; Genet, C.; et al. *Angew. Chem.* **2016**, *128*, 11634−11638.
(19) Flick, J.; Ruggenthaler, M.; Appel, H.; Rubio, A. *Proc. Natl. Acad. Sci. U. S. A.* **2017**, *114*, 3026−3034.
(20) Bennett, K.; Kowalewski, M.; Mukamel, S. *Faraday Discuss.* **2016**, *194*, 259−282.
(21) Bellessa, J.; Symonds, C.; Vynck, K.; Lemaitre, A.; Brioude, A.; Beaur, L.; Plenet, J.; Viste, P.; Felbacq, D.; Cambril, E.; et al. *Phys. Rev. B: Condens. Matter Mater. Phys.* **2009**, *80*, 33303.
(22) Zengin, G.; Johansson, G.; Johansson, P.; Antosiewicz, T. J.; Käll, M.; Shegai, T. *Sci. Rep.* **2013**, *3*, 3074.
(23) Schlather, A. E.; Large, N.; Urban, A. S.; Nordlander, P.; Halas, N. J. *Nano Lett.* **2013**, *13*, 3281−3286.
(24) Eizner, E.; Avayu, O.; Ditcovski, R.; Ellenbogen, T. *Nano Lett.* **2015**, *15*, 6215−6221.
(25) Fofang, N. T.; Park, T.-H.; Neumann, O.; Mirin, N. A.; Nordlander, P.; Halas, N. J. *Nano Lett.* **2008**, *8*, 3481−3487.
(26) Sugawara, Y.; Kelf, T.; Baumberg, J.; Abdelsalam, M.; Bartlett, P. *Phys. Rev. Lett.* **2006**, *97*, 266808.
(27) Eizner, E.; Ellenbogen, T. *Appl. Phys. Lett.* **2014**, *104*, 223301.
(28) Novotny, L.; Hecht, B. *Principles of Nano-Optics*; Cambridge University Press: Cambridge, U.K., 2012.
(29) Biagioni, P.; Huang, J.-S.; Hecht, B. *Rep. Prog. Phys.* **2012**, *75*, 24402.
(30) Grynberg, G.; Aspect, A.; Fabre, C. *Introduction to Quantum Optics: From the Semi-Classical Approach to Quantized Light*; Cambridge University Press: Cambridge, U.K., 2010.
(31) Langhammer, C.; Schwind, M.; Kasemo, B.; Zoric, I. *Nano Lett.* **2008**, *8*, 1461−1471.
(32) Olson, J.; Manjavacas, A.; Liu, L.; Chang, W.-S.; Foerster, B.; King, N. S.; Knight, M. W.; Nordlander, P.; Halas, N. J.; Link, S. *Proc. Natl. Acad. Sci. U. S. A.* **2014**, *111*, 14348−14353.
(33) Knight, M. W.; King, N. S.; Liu, L.; Everitt, H. O.; Nordlander, P.; Halas, N. J. *ACS Nano* **2014**, *8*, 834−840.
(34) Knight, M. W.; Liu, L.; Wang, Y.; Brown, L.; Mukherjee, S.; King, N. S.; Everitt, H. O.; Nordlander, P.; Halas, N. J. *Nano Lett.* **2012**, *12*, 6000−6004.
(35) McClain, M. J.; Schlather, A.; Ringe, E.; King, N. S.; Liu, L.; Manjavacas, A.; Knight, M.; Kumar, I.; Whitmire, K. H.; Everitt, H. O.; et al. *Nano Lett.* **2015**, *15*, 2751.
(36) Ellenbogen, T.; Seo, K.; Crozier, K. B. *Nano Lett.* **2012**, *12*, 1026−1031.
(37) Novotny, L.; van Hulst, N. *Nat. Photonics* **2011**, *5*, 83−90.
(38) Novotny, L. *Phys. Rev. Lett.* **2007**, *98*, 266802.
(39) van Burgel, M.; Wiersma, D. A.; Duppen, K. *J. Chem. Phys.* **1995**, *102*, 20−33.
(40) Saikin, S. K.; Eisfeld, A.; Valleau, S.; Aspuru-Guzik, A. *Nanophotonics* **2013**, *2*, 21−38.
(41) Bakalis, L. D.; Knoester, J. *J. Phys. Chem. B* **1999**, *103*, 6620−6628.
(42) Minoshima, K.; Taiji, M.; Misawa, K.; Kobayashi, T. *Chem. Phys. Lett.* **1994**, *218*, 67−72.
(43) Akselrod, G. M.; Tischler, Y. R.; Young, E. R.; Nocera, D. G.; Bulovic, V. *Phys. Rev. B: Condens. Matter Mater. Phys.* **2010**, *82*, 113106.
(44) Crut, A.; Maioli, P.; Del Fatti, N.; Vallée, F. *Phys. Rep.* **2015**, *549*, 1−43.
(45) Chang, W.-S.; Wen, F.; Chakraborty, D.; Su, M.-N.; Zhang, Y.; Shuang, B.; Nordlander, P.; Sader, J. E.; Halas, N. J.; Link, S. *Nat. Commun.* **2015**, *6*, 7022.
(46) Giannetti, C.; Revaz, B.; Banfi, F.; Montagnese, M.; Ferrini, G.; Cilento, F.; Maccalli, S.; Vavassori, P.; Oliviero, G.; Bontempi, E.; et al. *Phys. Rev. B: Condens. Matter Mater. Phys.* **2007**, *76*, 125413.
(47) Yu, K.; Zijlstra, P.; Sader, J. E.; Xu, Q.-H.; Orrit, M. *Nano Lett.* **2013**, *13*, 2710−2716.
(48) Su, M.-N.; Dongare, P. D.; Chakraborty, D.; Zhang, Y.; Yi, C.; Wen, F.; Chang, W.-S.; Nordlander, P.; Sader, J. E.; Halas, N. J.; et al. *Nano Lett.* **2017**, *17*, 2575−2583.
(49) Lin, K.-H.; Lai, C.-M.; Pan, C.-C.; Chyi, J.-I.; Shi, J.-W.; Sun, S.-Z.; Chang, C.-F.; Sun, C.-K. *Nat. Nanotechnol.* **2007**, *2*, 704−708.
(50) Dacosta Fernandes, B.; Spuch-Calvar, M.; Baida, H.; Tréguer-Delapierre, M.; Oberlé, J.; Langot, P.; Burgin, J. *ACS Nano* **2013**, *7*, 7630−7639.
(51) Feng, X. L.; White, C. J.; Hajimiri, A.; Roukes, M. L. *Nat. Nanotechnol.* **2008**, *3*, 342−346.
(52) Bonnand, C.; Bellessa, J.; Plenet, J. *Phys. Rev. B: Condens. Matter Mater. Phys.* **2006**, *73*, 245330.
(53) Simon, T.; Melnikau, D.; Sánchez-Iglesias, A.; Grzelczak, M.; Liz-Marzán, L. M.; Rakovich, Y.; Feldmann, J.; Urban, A. S. *J. Phys. Chem. C* **2016**, *120*, 12226−12233.
(54) Wersäll, M.; Cuadra, J.; Antosiewicz, T. J.; Balci, S.; Shegai, T. *Nano Lett.* **2017**, *17*, 551−558.
(55) Melnikau, D.; Esteban, R.; Savateeva, D.; Sánchez-Iglesias, A.; Grzelczak, M.; Schmidt, M. K.; Liz-Marzán, L. M.; Aizpurua, J.; Rakovich, Y. P. *J. Phys. Chem. Lett.* **2016**, *7*, 354−362.
(56) Schwartz, T.; Hutchison, J. A.; Léonard, J.; Genet, C.; Haacke, S.; Ebbesen, T. W. Polariton. *ChemPhysChem* **2013**, *14*, 125−131.
(57) Virgili, T.; Coles, D.; Adawi, A. M.; Clark, C.; Michetti, P.; Rajendran, S. K.; Brida, D.; Polli, D.; Cerullo, G.; Lidzey, D. G. *Phys. Rev. B: Condens. Matter Mater. Phys.* **2011**, *83*, 245309.

DOI: 10.1021/acs.nanolett.7b03751
Nano Lett. 2017, 17, 7675−7683

(58) Song, J.-H.; He, Y.; Nurmikko, A. V.; Tischler, J.; Bulovic, V. *Phys. Rev. B: Condens. Matter Mater. Phys.* **2004**, *69*, 235330.
(59) Hao, Y.-W.; Wang, H.-Y.; Jiang, Y.; Chen, Q.-D.; Ueno, K.; Wang, W.-Q.; Misawa, H.; Sun, H.-B. *Angew. Chem.* **2011**, *123*, 7970−7974.
(60) Balci, S.; Kocabas, C.; Küçüköz, B.; Karatay, A.; Akhüseyin, E.; Gul Yaglioglu, H.; Elmali, A. *Appl. Phys. Lett.* **2014**, *105*, 51105.
(61) Balci, S.; Kucukoz, B.; Balci, O.; Karatay, A.; Kocabas, C.; Yaglioglu, G. *ACS Photonics* **2016**, *3*, 2010−2016.
(62) Vasa, P.; Pomraenke, R.; Cirmi, G.; De Re, E.; Wang, W.; Schwieger, S.; Leipold, D.; Runge, E.; Cerullo, G.; Lienau, C. *ACS Nano* **2010**, *4*, 7559−7565.
(63) Wang, W.; Vasa, P.; Pomraenke, R.; Vogelgesang, R.; De Sio, A.; Sommer, E.; Maiuri, M.; Manzoni, C.; Cerullo, G.; Lienau, C. *ACS Nano* **2014**, *8*, 1056−1064.
(64) Wang, H.; Wang, H.-Y.; Bozzola, A.; Toma, A.; Panaro, S.; Raja, W.; Alabastri, A.; Wang, L.; Chen, Q.-D.; Xu, H.-L.; Angelis, F. D.; Sun, H.-B.; Zaccaria, R. P. *Adv. Funct. Mater.* **2016**, *26*, 6198−6206.
(65) Wu, X.; Gray, S. K.; Pelton, M. *Opt. Express* **2010**, *18*, 23633.
(66) Mukherjee, S.; Sobhani, H.; Lassiter, J. B.; Bardhan, R.; Nordlander, P.; Halas, N. J. *Nano Lett.* **2010**, *10*, 2694−2701.
(67) Rodriguez, S. R. K.; Abass, A.; Maes, B.; Janssen, O. T. A.; Vecchi, G.; Gómez Rivas, J. *Phys. Rev. X* **2011**, *1*, 21019.
(68) Garrido Alzar, C. L.; Martinez, M. A. G.; Nussenzveig, P. *Am. J. Phys.* **2002**, *70*, 37−41.
(69) Novotny, L. *Am. J. Phys.* **2010**, *78*, 1199−1202.
(70) Rudin, S.; Reinecke, T. L. *Phys. Rev. B: Condens. Matter Mater. Phys.* **1999**, *59*, 10227−10233.

DOI: 10.1021/acs.nanolett.7b03751
Nano Lett. 2017, 17, 7675−7683